Supplementary Information

High yield production of 3-hydroxypropionic acid using *Issatchenkia orientalis*

Tan et al.

Table of content

Supplementary Methods

Supplementary Method 1. qPCR analysis

Engineered strains were inoculated in YPAD medium and grown at 30 °C with constant shaking at 200 rpm overnight. The cells were then subcultured into fresh YP medium with 20 g/L glucose with the initial OD_{600} of 0.2 and grown until the OD_{600} reached 1. Cells were collected from 1 mL of culture, and total RNA was extracted using the RNeasy mini kit from Qiagen (Valencia, CA). cDNA synthesis was performed using the iScript™ Reverse Transcription Supermix from Biorad, and iTaq Universal SYBR Green Supermix from Biorad was used for qPCR following the manufacturer's protocol. Primers for qPCR were designed using the IDT online tool (Primer Quest). The endogenous gene *alg9*, encoding a mannosyltransferase, was used as the internal control. Expression of the selected gene was normalized by the *alg9* expression level. Raw data was analyzed using QuantStudioTM Real-time PCR software from Applied Biosystems. qPCR analysis was performed with technical triplicates.

Supplementary Method 2. Scenarios simulated for techno-economic analysis (TEA) and life cycle assessment (LCA)

Dextrose-accepting biomanufacturing facilities were simulated under alternative fermentation scenarios with assumptions for yield, titer, and productivity corresponding to the fermentation performance achieved in this study in the 100 mL DASbox (*DASbox dextrose scenario*). A bioreactor working volume fraction of 33% was assumed in all scenarios based on the working volume fraction used in the DASbox experiments. The mass transfer properties and effects of gas sparging can be tightly coupled with reactor design parameters such as the reactor headspace volume.[1] Therefore, although this working volume fraction is substantially lower than bioreactor working volume fractions assumed in previous TEAs (e.g., 80%),[2] we wanted to use a working volume fraction consistent with that used in our experiments to conservatively represent the current state-of-technology under *n*th plant assumptions. Changing the fermentation working volume fraction to that assumed in previous TEAs (e.g., 80%−90%),[2,3] would moderately change TEA results (MPSP, TCI, and AOC decreased by 4.8−5.3%, 16.8−18.2%, and 1.1−1.2%, respectively) and would not substantially influence LCA results (CI and FEC decreased by 0.2−0.2% and 0.3−0.3%, respectively, in the *dextrose scenario*; **Supplementary Figure 23**). Further, to assess the system sustainability implications of potential alternative feedstocks, we designed end-to-end biomanufacturing facilities that could accept corn, sugarcane, and corn stover as feedstocks, and simulated them under assumptions corresponding to the fermentation performance achieved in this study using dextrose in the DASbox (*corn*, *sugarcane*, and *corn stover scenarios*, respectively; assumed baseline values and distributions for all uncertain parameters in each scenario are reported in **Supplementary Data 1**).

Supplementary Method 3. Plasmid construction

Plasmids for gene overexpression were generated by the *in vivo* DNA assembly method in *S. cerevisiae* or Gibson assembly in *E. coli*. For DNA assembly, 50~100 ng of PCR-amplified fragments and restriction enzyme digested backbone were co-transformed into *S. cerevisiae* via lithium acetate-mediated method. All colonies formed on SC-URA plates were collected. Plasmids were extracted from *S. cerevisiae* and retransformed into *E. coli*. Plasmids from several *E. coli* colonies were extracted and verified by restriction digestion. Strong promoters and terminators identified previously were chosen for gene overexpression. To construct plasmids for gene deletion, gBlocks containing homology donors and spacers were synthesized by Integrated DNA Technologies. The homology donor contained two 50 bp homology arms flanking the Cas9 cutting site, and a restriction enzyme, such as *Xho*I, was in the middle of the two homology arms. The gBlocks were then cloned into the CRISPR/Cas9 plasmid by Golden Gate assembly. Detailed construction of each plasmid is described as following:

pTM-*PAND(1-9)*. The primer pairs of P(1-9)*PGK1t*-F and *ura3PGK1t*-R were used to amplify for *PGK1t*, *PGK1tura3p*-F and *TDH3pPDC1t*-R for the backbone, *PDC1tTDH3p*-F and *TDH3p*P(1-9)-R for *TDH3p*, and for the *PAND* genes, *PAND(1-9)*-F and *PAND(1-9)*-R. DNA assembler was used to assemble the PCR products to generate the plasmids pTM_*PAND(1-9)*.

pTM-*BAPAT(1-7)*. The primer pairs of B(1-7)*Trp3t*-F and *Trp3tura3*-R were used to amplify *Trp3t*, *Trp3tura3*-F and *GPM1PDC1t*-R for the backbone, *GPM1PDC1t*-F and *GPM1*B(1-7)-R for *GPM1*, and for the *BAPAT* genes, *BAPAT(1-7)*-F and *BAPAT*HIS-R. DNA assembler was used to assemble the PCR products to make pTM_*BAPAT(1-7)*.

PTM_*YDFG(1-10)*. The primers pairs of Y(1-10)*FBA1p*-F and *ura3FBA1p*-R were used to amplify *FBA1p*, *FBA1pura3*-F and *ENO2tPDC1t*-R were used to amplify the backbone, *PDC1tENO2t*-F and Y(1-10)*ENO2t*-R were used to amplify *ENO2t*, and for the *YDFG* genes, *YDFG(1-10)*-F and *YDFG(1-10)*-R were used. DNA assembler was used to assemble the PCR products to generate the plasmids pTM_*YDFG(1-10)*.

pPBY. *PAND5* gene cassette was amplified from pTM-*PAND5* using primer pairs of LP10-*TDH3p*-F and *GPMp*-pTM-common-R. *BAPAT6* gene cassette was amplified from pTM-*BAPAT6* using primer pairs of pTM-*GPMp*-F and *FBAp-Trp3t*-R. *YDFG3* gene cassette was amplified from pTM-*YDFG3* using primer pairs of *Trp3t-FBAp*-F and LP10-*ENO2t*-R. The backbone pHT was linearized by 3HPBG-pZF-F and 3HPBG-pZF-R. After obtaining four fragments, DNA assembly was used to assemble fragments

pHT-*AAT2*. *IoAAT2* was amplified from *I. orientalis* genomic DNA using primer pairs of GA-*g963*-F and GA-*g693*-R. pHT backbone containing GPM promoter and Eno2 terminator was linearized by primer pairs of GA-pZF-F and GA-pZF-R. After obtaining the two fragments, HIFI assembly was used to assemble fragments.

Supplementary Method 4. Strain construction

For gene deletion, CRISPR/Cas9 plasmid was transformed to *I. orientalis* via a lithium acetate-mediated method, and transformants were plated on an SC-URA plate and incubated at 30 ºC. Several colonies were randomly picked and cultivated in liquid SC-URA medium. Then, colony PCR was performed or then restriction digestion was performed to verify the deletion. For gene overexpression, the cassette for gene overexpression was PCR-amplified to contain 40 bp to 42 bp homology arms flanking the integration site. The PCR product and CRISPR/Cas9 plasmid targeting the integration site were co-transformed to *I. orientalis* via the lithium acetate-mediated method. Transformants were plated on an SC-URA plate and incubated at 30 ºC. Several colonies were randomly picked and cultivated in liquid YPAD medium. Then, colony PCR was performed for verifying gene overexpression. Plasmid removal was performed using FOA selection. Detailed construction of each strain is described as following:

PBY1/*ura3*Δ. EG14-LHR-F and EG14-LHR-R were used to amplify the PBY expression cassette from pPBY. Amplified product and pVT36b-EG14 plasmid were then transformed into SD108/*ura3*Δ.

PBY2/*ura3*Δ. EG15-LHR-F and EG15-LHR-R were used to amplify the PBY expression cassette from pPBY. Amplified product and pVT36b-EG15 plasmid were then transformed into PBY1/*ura3*Δ.

PBY3/*ura3*Δ. EG2-LHR-F and EG15-LHR-R were used to amplify the PBY expression cassette from pPBY. Amplified product and pVT36b-EG2 plasmid were then transformed into PBY2/*ura3*Δ.

1P/*ura3*Δ. EG9-LHR-F and EG9-LHR-F were used amplified the *PAND5* expression cassette from pTM-*PAND5*. Amplified product and pVT36b-EG9 plasmid were then transformed into LPB/*ura3*Δ.

1P/*ura3*Δ. EG8-LHR-F and EG8-LHR-F were used amplified the *PAND5* expression cassette from pTM-*PAND5*. Amplified product and pVT36b-EG8 plasmid were then transformed into LPB/*ura3*Δ.

2P/*ura3*Δ. EG4-LHR-F and EG4-LHR-F were used amplified the *PAND5* expression cassette from pTM-*PAND5*. Amplified product and pVT36b-EG4 plasmid were then transformed into LPB/*ura3*Δ.

3P/*ura3*Δ. EG6-LHR-F and EG6-LHR-F were used amplified the *PAND5* expression cassette from pTM-*PAND5*. Amplified product and pVT36b-EG6 plasmid were then transformed into LPB/*ura3*Δ.

4P/*ura3*Δ. GD11-LHR-F and GD11-LHR-F were used amplified the *PAND5* expression cassette from pTM-*PAND5*. Amplified product and pVT36b- GD11 plasmid were then transformed into LPB/*ura3*Δ.

5P/*ura3*Δ. GD27-LHR-F and GD27-LHR-F were used amplified the *PAND5* expression cassette from pTM-*PAND5*. Amplified product and pVT36b- GD27 plasmid were then transformed into LPB/*ura3*Δ.

6P/*ura3*Δ. EG8-LHR-F and EG8-LHR-F were used amplified the *PAND5* expression cassette from pTM-*PAND5*. Amplified product and pVT36b-EG8 plasmid were then transformed into 5P/*ura3*Δ.

7P/*ura3*Δ. EG4-LHR-F and EG4-LHR-F were used amplified the *PAND5* expression cassette from pTM-*PAND5*. Amplified product and pVT36b-EG4 plasmid were then transformed into 5P/*ura3*Δ.

8P/*ura3*Δ. EG6-LHR-F and EG6-LHR-F were used amplified the *PAND5* expression cassette from pTM-*PAND5*. Amplified product and pVT36b-EG6 plasmid were then transformed into 5P/*ura3*Δ.

8P/*ura3*Δ/*pdc*Δ. pVT36b-*pcd* which contained the homology arm targeting to *pdc* gene was transformed into 8P/*ura3*Δ.

8P/*ura3*Δ/*pdc*Δ/*gpd*Δ. The upstream and downstream sequences of *gpd* were amplified from I. orientalis genomic DNA. Primer pairs of *GPD*-seq-F and *GPD*-KO-Up-R were used for upstream sequence. Primer pairs of *GPD*-KO-Down-F and *GPD*-seq-R were used for downstream sequence. pVT36b-*gpd*, upstream sequence and downstream sequence were transformed into 8P/*ura3*Δ/*pdc*Δ.

8P-AP/*ura3*Δ/*pdc*Δ/*gpd*Δ. Primer pairs of EG8-*FBA1p-IoPYC*-F and GPMp-*TEFt-IoPYC*-R were used to amplify the IoPYC expression cassette from pRS416-SA-site1. Primers pairs of *TEF1t-GPMp*-F and EG8-*ENO2t* (pZF)-R were used to amplify the *AAT2* expression cassette from pHT-*AAT2*. pVT36b-EG8 and fragments of the *IoPYC* expression cassette and the *AAT2* expression cassette were transformed into 8P/*ura3*Δ/*pdc*Δ/*gpd*Δ.

1AP/*ura3*Δ. Primer pairs of EG16-LHR-F and EG16-LHR-F were used to amplify the *BAPAT* and *YDFG* expression cassette from pBY. Amplified product and pVT36b-EG16 plasmid were then transformed into 8P-AP/*ura3*Δ/*pdc*Δ/*gpd*Δ.

2AP/*ura3*Δ. Primer pairs of EG17-*FBA1p-IoPYC*-F and GPMp-*TEFt-IoPYC*-R were used to amplify the *IoPYC* expression cassette from pRS416-SA-site1. Primers pairs of *TEF1t-GPMp*-F and EG17-*ENO2t* (pZF)-R were used to amplify the *AAT2* expression cassette from pHT-AAT2. pVT36b-EG17 and fragments of the IoPYC expression cassette and the *AAT2* expression cassette were transformed into 1AP/*ura3*Δ

2AP. Primer pairs of *ura3*-F and *ura3*-R were used to amplify the *ura3* expression cassette from pVT101a. The *ura3* expression cassette was further transformed to 2AP/*ura3*Δ.

Supplementary Method 5. Sequence Similarity Network (SSN) analysis

SSN analysis was performed for *PAND*, *BAPAT* and *YDFG* gene to get candidates of each gene (https://efi.igb.illinois.edu/efi-est/)[4]. For *PAND* gene, *PAND* gene from *T. castaneum* was input into the

SSN analysis. For *BAPAT* gene, *BAPAT* from *B. cereus*. For *YDFG* gene, *YDFG* gene from *E. coli* was input into the SSN analysis. All the candidate genes were randomly picked in different cluster after SSN analysis.

.

Supplementary Tables

Supplementary Table 1. Thermodynamic analysis of the β-alanine pathway

RxnID	Gene	Reaction Name	$\Delta_rG'°$, pH7 eQuilibrator	$\Delta_rG'°$, pH6 eQuilibrator
PC_c	*PYC*	pyruvate carboxylase	–5.90 ± 1.40	−1.72 ± 1.40
ASPTA_c	*AAT*	aspartate transaminase	2.80 ± 1.10	3.16 ± 1.10
ASP1DC_c	*PAND*	aspartate 1-decarboxylase	–17.30 ± 11.70	−28.06 ± 11.70
3A2OA_c	*BAPAT*	beta-alanine-pyruvate aminotransferase	–3.90 ± 5.80	−3.27 ± 5.80
MSAR_c	*YDFG*	malonic semialdehyde reductase	–21.20 ± 5.70	−29.66 ± 5.70

Reaction IDs (RxnID) and gene abbreviations are as in Table 1 of the text.

Data presents the estimated changes in Gibbs free energy, **$\Delta_rG'°$** (kJ/mole) ± standard error (kJ/mole) with both values calculated using the eQuilibrator computational tool.

Supplementary Table 2. Feeding profile in the fed-batch fermentation

	300 mL
First feeding	8.5 mL at 24 hr
Second feeding	12.5 mL at 48 hr
Third feeding	10 mL at 96 hr
Fourth feeding	N.A.
Final Titer (g/L)	92.0
Yield (g/g)*	0.70
Productivity (g/L/hr)	0.548

P.S. Feeding solution for three scales is 590-600 g/L glucose.

* Yield = Sum of 3HP produced in each feeding/ Total glucose consumed

Supplementary Table 3. Benchmark of 3HP production using different hosts and different pathways.

Strain	Pathway	Titer (g/L)	Yield (g/g)	Productivity (g/L/hr)	Carbon	pH control	Refs
K. pneumoniae	Glycerol	**102.6**	0.43	1.07	MM with glycerol and yeast extract	pH 7.0	[5]
E. coli	Glycerol	76.2	0.46	**1.89**	MM with glycerol and yeast extract	pH 7.0	[6]
S. cerevisiae	Mitochondria Malonyl-CoA	71.1	0.23	0.71	MM with glucose	pH 5.0	[7]
S. cerevisiae	Cytosol Malonyl-CoA	56.5	0.31	0.53	MM with glucose	pH 5.6	[8]
S. cerevisiae	Cytosol Malonyl-CoA	11.3	0.56	N.A.	MM with Glucose	With Calcium carbonate	[9]
P. pastoris	Cytosol Malonyl-CoA	48.2	0.23	0.16	MM with Methanol	pH 5.6	[10]
R. toruloides	Cytosol Malonyl-CoA	45.2	0.11	0.44	MM with Lignocellulosic hydrolysate	No	[11]
O. polymorpha	Cytosol Malonyl-CoA	79.6	0.35	0.40	MM with xylose and glucose	pH 5.6	[12]
Y. lipolytica	Cytosol Malonyl-CoA	100	0.2	0.48	MM with glucose	pH 6.0	[13]
S. cerevisiae	β-alanine	13.7	0.14	0.17	MM with glucose	pH 5.0	[14]
E. coli	β-alanine	72.2	0.6	1.64	Semi-MM (15 g/L yeast extract) with glycerol	pH 6.5	[15]

Supplementary Table 4. Strains used in this study.

Strains	Features	Sources
E. coli DH5α	Cloning host	NEB
SD108/*ura3*Δ	*I. orientalis* SD108 with uracil autotrophy	[16]
LPB/*ura3*Δ	SD108/*ura3*Δ with landing pad integration	[17]
pPBY/PBY1/*ura3*Δ	P5B6Y3 integrated to the *EG14* site in SD108/*ura3*Δ with pPBY plasmid	This study
pPBY/PBY2/*ura3*Δ	P5B6Y3 integrated to the *EG15* site in PBY1/*ura3*Δ with pPBY plasmid	This study
pPBY/PBY3/*ura3*Δ	P5B6Y3 integrated to the *EG2* site in PBY2/*ura3*Δ with pPBY plasmid	This study
pPBY/1P/*ura3*Δ	*PAND5* integrated to LPB/*ura3*Δ at *EG8* with pPBY plasmid	This study
pPBY/2P/*ura3*Δ	*PAND5* integrated to LPB/*ura3*Δ at *EG4* with pPBY plasmid	This study
pPBY/3P/*ura3*Δ	*PAND5* integrated to LPB/*ura3*Δ at EG6 with pPBY plasmid	This study
pPBY/4P/*ura3*Δ	*PAND5* integrated to LPB/*ura3*Δ at GD11 with pPBY plasmid	This study
pPBY/5P/*ura3*Δ	*PAND5* integrated to LPB/*ura3*Δ at GD27 with pPBY plasmid	This study
pPBY/6P/*ura3*Δ	*PAND5* integrated to pPBY/5P/*ura3*Δ at EG8 with pPBY plasmid	This study
pPBY/7P/*ura3*Δ	*PAND5* integrated to pPBY/5P/*ura3*Δ at EG4 with pPBY plasmid	This study
pPBY/8P/*ura3*Δ	*PAND5* integrated to pPBY/5P/*ura3*Δ at EG6 with pPBY plasmid	This study
pPBY/8P/*ura3*Δ/*pdc*Δ	pPBY/8P/*ura3*Δ with *pdc* knockout	This study
pPBY/8P/*ura3*Δ/*pdc*Δ/*gpd*Δ	pPBY/8P/*ura3*Δ/*pdc*Δ with *gpd* knockout	This study
pPBY/8P-AP/*ura3*Δ/*pdc*Δ/*gpd*Δ	pPBY/8P/*ura3*Δ/*pdc*Δ/*gpd*Δ with *PYC-AAT2* integrated to EG8	This study
1AP/*ura3*Δ	8P-AP/*ura3*Δ/*pdc*Δ/*gpd*Δ with *BAPAT6* and *YDFG3* integrated to EG16	This study
pHT/1AP/*ura3*Δ	1AP/*ura3*Δ with pHT plasmid	This study
pPBY/1AP/*ura3*Δ	1AP/*ura3*Δ with pPBY plasmid	This study
2AP/*ura3*Δ	1AP/*ura3*Δ with PYC-*AAT2* integrated to EG17	This study
2AP	2AP/*ura3*Δ with *ura3* recovered	This study

Supplementary Table 5. Plasmids used in this study.

Plasmids	Features	Sources
pVT36b	*I. orientalis* plasmid for gene deletion and insertion	[18]
pVT36b-EG2	pVT36b with insertion of spacer for integration at site *EG2*	[17]
pVT36b-EG4	pVT36b with insertion of spacer for integration at site *EG4*	[17]
pVT36b-EG6	pVT36b with insertion of spacer for integration at site *EG6*	[17]
pVT36b-EG8	pVT36b with insertion of spacer for integration at site *EG8*	[17]
pVT36b-EG9	pVT36b with insertion of spacer for integration at site *EG9*	[17]
pVT36b-EG14	pVT36b with insertion of spacer for integration at site *EG14*	[17]
pVT36b-EG15	pVT36b with insertion of spacer for integration at site *EG15*	[17]
pVT36b-EG16	pVT36b with insertion of spacer for integration at site *EG16*	[17]
pVT36b-EG17	pVT36b with insertion of spacer for integration at site *EG17*	[17]
pVT36b-GD5	pVT36b with insertion of spacer for integration at site *GD5*	[17]
pVT36b-GD11	pVT36b with insertion of spacer for integration at site *GD11*	[17]
pVT36b-GD21	pVT36b with insertion of spacer for integration at site *GD21*	[17]
pVT36b-GD27	pVT36b with insertion of spacer for integration at site *GD27*	[17]
pVT36b-*pdc*	pVT36b with insertion of spacer for deletion of *pdc* with 50 bp upstream and downstream homology arm targeting to *pdc* gene	[19]
pVT36b-*gpd*	pVT36b with insertion of spacer for deletion of *gpd*	[19]
pRS416-SA-site1	pRS416 harboring reductive TCA pathway flanked with homology arms for integration to site 1	[19]
pVT101a	*I. orientalis* plasmid for gene deletion and insertion	[19]
pTM-*PAND1*	pTM with insertion of *TDH3p-PAND1-PGK1t*	This study
pTM-*PAND2*	pTM with insertion of *TDH3p-PAND2-PGK1t*	This study
pTM-*PAND3*	pTM with insertion of *TDH3p-PAND3-PGK1t*	This study
pTM-*PAND4*	pTM with insertion of *TDH3p-PAND4-PGK1t*	This study
pTM-*PAND5*	pTM with insertion of *TDH3p-PAND5-PGK1t*	This study
pTM-*PAND6*	pTM with insertion of *TDH3p-PAND6-PGK1t*	This study
pTM-*PAND7*	pTM with insertion of *TDH3p-PAND7-PGK1t*	This study
pTM-*PAND8*	pTM with insertion of *TDH3p-PAND8-PGK1t*	This study
pTM-*BAPAT1*	pTM with insertion of *GPMp-BAPAT1-Trp3t*	This study
pTM-*BAPAT2*	pTM with insertion of *GPMp-BAPAT2-Trp3t*	This study
pTM-*BAPAT3*	pTM with insertion of *GPMp-BAPAT3-Trp3t*	This study
pTM-*BAPAT4*	pTM with insertion of *GPMp-BAPAT4-Trp3t*	This study
pTM-*BAPAT5*	pTM with insertion of *GPMp-BAPAT5-Trp3t*	This study
pTM-*BAPAT6*	pTM with insertion of *GPMp-BAPAT6-Trp3t*	This study
pTM-*BAPAT7*	pTM with insertion of *GPMp-BAPAT7-Trp3t*	This study
pTM-*YDFG1*	pTM with insertion of *FBA1p-YDFG1-ENO2t*	This study
pTM-*YDFG2*	pTM with insertion of *FBA1p-YDFG2-ENO2t*	This study
pTM-*YDFG3*	pTM with insertion of *FBA1p-YDFG3-ENO2t*	This study
pTM-*YDFG4*	pTM with insertion of *FBA1p-YDFG4-ENO2t*	This study
pTM-*YDFG5*	pTM with insertion of *FBA1p-YDFG5-ENO2t*	This study
pTM-*YDFG6*	pTM with insertion of *FBA1p-YDFG6-ENO2t*	This study
pTM-*YDFG7*	pTM with insertion of *FBA1p-YDFG7-ENO2t*	This study
pTM-*YDFG8*	pTM with insertion of *FBA1p-YDFG8-ENO2t*	This study
pTM-*YDFG9*	pTM with insertion of *FBA1p-YDFG9-ENO2t*	This study
pTM-*YDFG10*	pTM with insertion of *FBA1p-YDFG10-ENO2t*	This study
pPBY	pHT with insertion of *TDH3p-PAND5-PGK1t-GPMp-BAPAT6-Trp3t-FBA1p-YDFG3-ENO2t*	This study
pHT-*AAT2*	pHT with insertion of *GPMp-IoAAT2-ENO2t*	This study

Supplementary Table 6. Details of the DasBox reactor

Parameter	**Lab Scale**
Manufacturer	Eppendorf DASbox
Nominal Volume (L)	0.3
Maximum Working Volume According to the Manufacture (L)	0.25
Actual Working Volume (L)	0.1
Tank Diameter (D_T, mm)	90
Tank Height (H_T, mm)	360
Impeller Type	6 blade Rushton
Impeller Diameter (D_I, mm)	30
Number of impellers	2
H_T/D_T	4
D_I/D_T	0.33
Aeration Rate (vvm)	2.4 sLPH
Stirrer Speed (RPM)	400-1200 (Cascaded on DO)

Supplementary Table 7. Breakdown of the *dextrose scenario* baseline biomanufacturing facility's total capital cost. *ISBL* and OSBL denote inside and outside battery limits, respectively.

Cost category	**Notes**	**Cost** (MM$)
	Direct costs	
ISBL installed equipment cost	-	134.12
OSBL installed equipment cost	-	62.30
Warehouse	4.0% of ISBL	5.36
Site development	9.0% of ISBL	12.07
Additional piping	4.5% of ISBL	6.04
Total direct cost (TDC)	-	219.88
	Indirect costs	
Pro-ratable costs	10.0% of TDC	21.99
Field expenses	10.0% of TDC	21.99
Construction	20.0% of TDC	43.98
Contingency	10.0% of TDC	21.99
Other indirect costs (start-up, permits, etc.)	10.0% of TDC	21.99
Total indirect cost (TIDC)	-	131.93
	Total capital investment	
Fixed capital investment (FCI)	*TDC + TIDC*	351.82
Working capital (WC)	5.0% of FCI	17.59
Total capital investment (TCI)	*FCI + WC*	369.41

Supplementary Table 8. Breakdown of the *dextrose scenario* baseline biomanufacturing facility's fixed operating cost. *ISBL* and OSBL denote inside and outside battery limits, respectively.

Cost category	**Notes**	**Cost** (MM$/y)
Labor salary	-	1.82
Labor burden	90% of labor salary	1.64
Maintenance	3.0% of ISBL	4.02
Property insurance	0.7% of ISBL	2.46
Total fixed operating cost (FOC)	-	1.82

Supplementary Figures

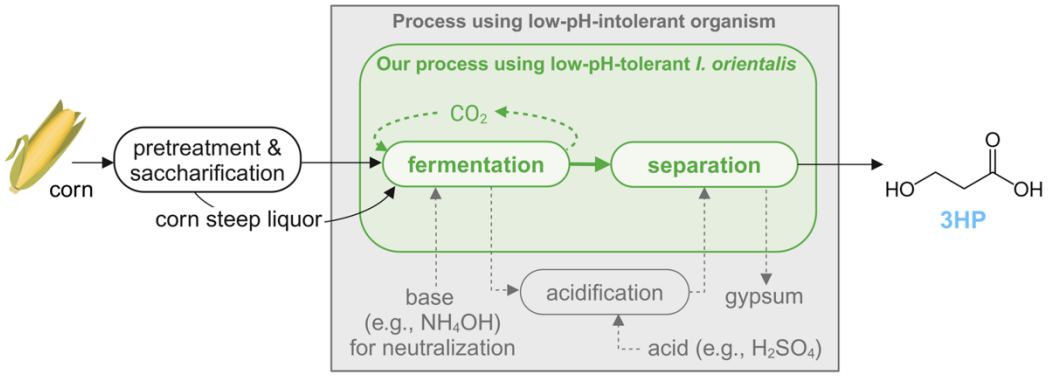

Supplementary Figure 1. Our engineered stain can survive readily at low pH and simultaneously produce 3HP, avoiding the need to neutralize the medium for cell growth and to re-acidulate 3HP downstream, facilitating low-cost and environmentally beneficial 3HP production. Created in BioRender. Zhao, H. (2025) https://BioRender.com/vkz7w01.

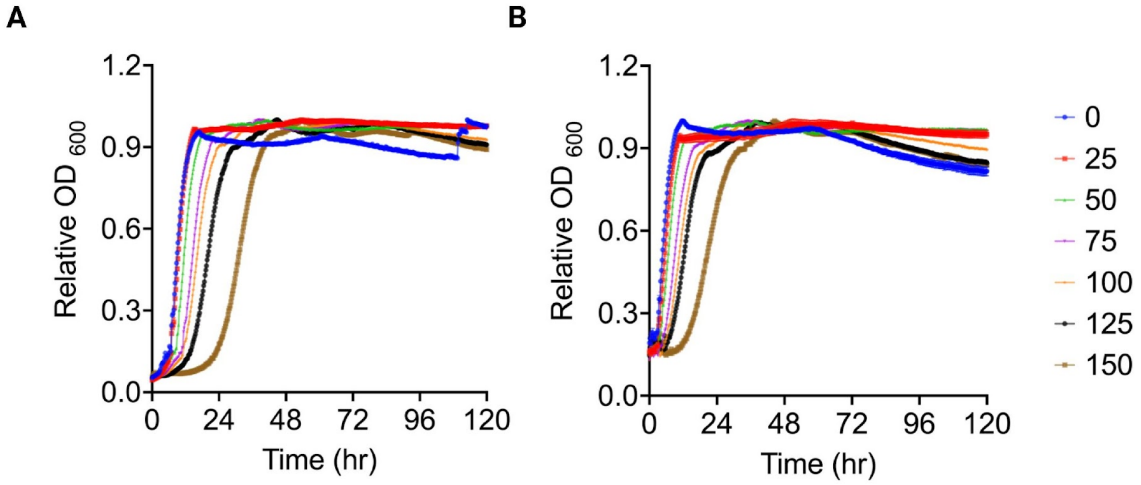

Supplementary Figure 2. 3HP tolerance tests. (A) a starting OD of 0.1 and (B) a starting OD of 1. Data present mean ± S.D. of three biologically independent samples (n = 3). Source data for this figure is available in the Source Data file. The initial pH was set at 5.6. Each curve was normalized by the highest OD obtained from individual replicate. As shown in Supplementary Figure 1A, the cells began to grow slowly as the 3HP concentration increased to 50 g/L, and a concentration of 150 g/L delayed exponential growth by one day. However, higher levels of 3HP typically occurred only at high ODs during the fermentation process. Therefore, we tested an initial OD of 1 (Supplementary Figure 1B), which showed no significant growth retardation when cells were grown in medium with up to 125 g/L of 3HP. Although there was a 12-hour delay in reaching the exponential growth phase using a medium supplemented with 150 g/L 3HP, starting with a higher OD effectively mitigated the toxicity from high levels of 3HP (i.e., up to 125 g/L).

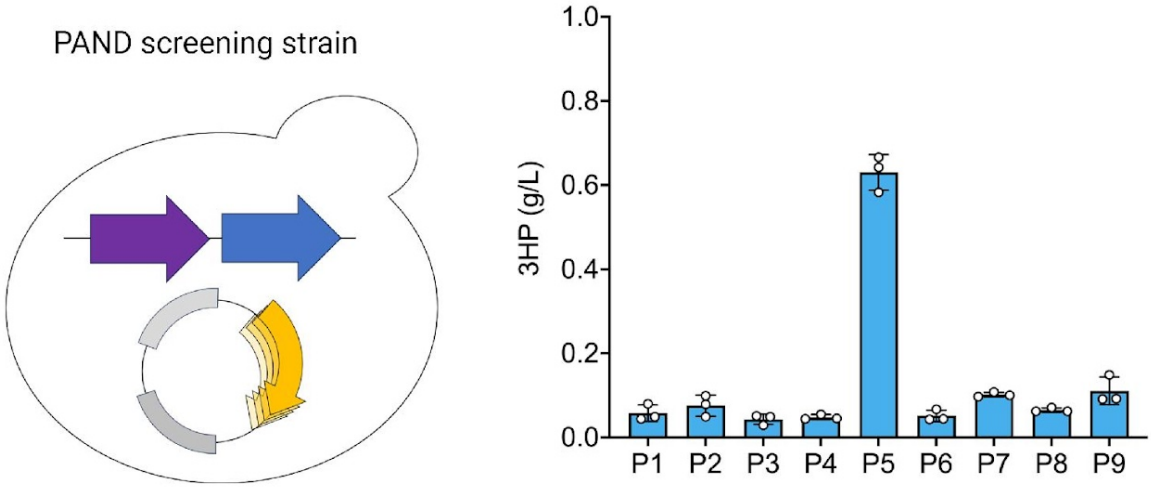

Supplementary Figure 3. *In vivo* test for *PAND* gene screening. *BcBAPAT* (purple color) and *EcYDFG* (blue color) were integrated to SD108 first to create the *PAND* screening strain and *PAND* gene candidate plasmids were transformed into *PAND* screening strain. Each strain with different *PAND* candidate plasmid was cultured in SC-URA with 50 g/L glucose for 5 days and 3HP was measured. Data present mean ± S.D. of three biologically independent samples (n = 3). Source data for this figure is available in the Source Data file. Created in BioRender. Zhao, H. (2025) https://BioRender.com/vkz7w01.

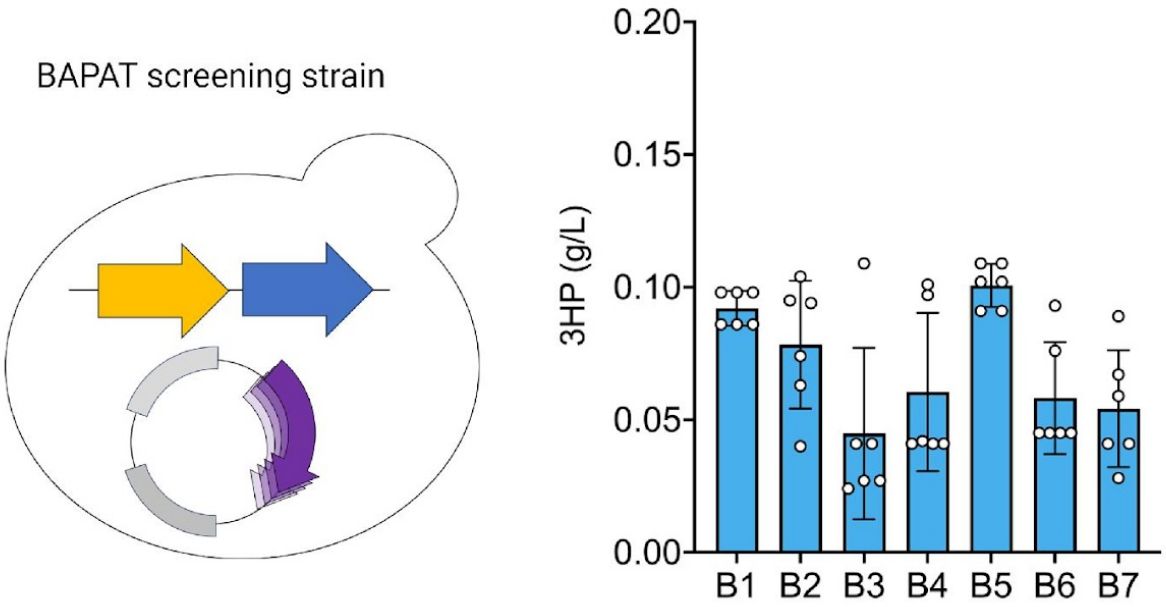

Supplementary Figure 4. *In vivo* test for *BAPAT* gene screening. *TcPAND* (yellow color) and *EcYDFG* (blue color) were integrated to SD108 first to create the *BAPAT* screening strain and *BAPAT* gene candidate plasmids were transformed into *BAPAT* screening strain. Each strain with different *PAND* candidate plasmid was cultured in SC-URA with 50 g/L glucose for 5 days and 3HP was measured. Data present mean ± S.D. of six biologically independent samples (n = 6). Source data for this figure is available in the Source Data file. Created in BioRender. Zhao, H. (2025) https://BioRender.com/vkz7w01.

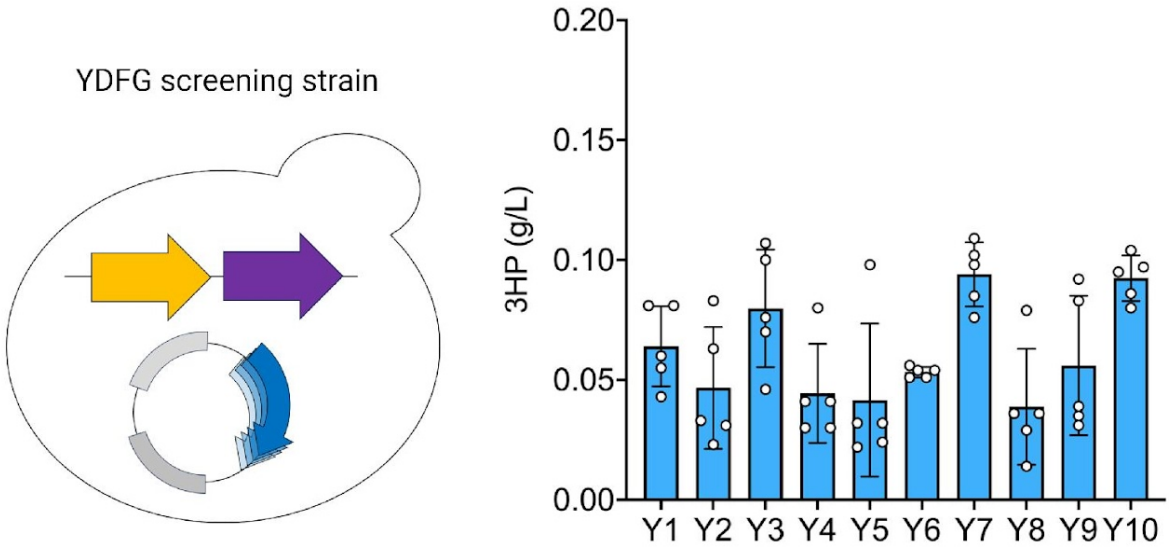

Supplementary Figure 5. *In vivo* test for *YDFG* gene screening. *TcPAND* (yellow color) and *BsBAPAT* (purple color) were integrated to SD108 first to create the *YDFG* screening strain and *YDFG* gene candidate plasmids were transformed into *YDFG* screening strain. Each strain with different *YDFG* candidate plasmid was cultured in SC-URA with 50 g/L glucose for 5 days and 3HP was measured. Data present mean ± S.D. of five biologically independent samples (n = 5). Source data for this figure is available in the Source Data file. Created in BioRender. Zhao, H. (2025) https://BioRender.com/vkz7w01.

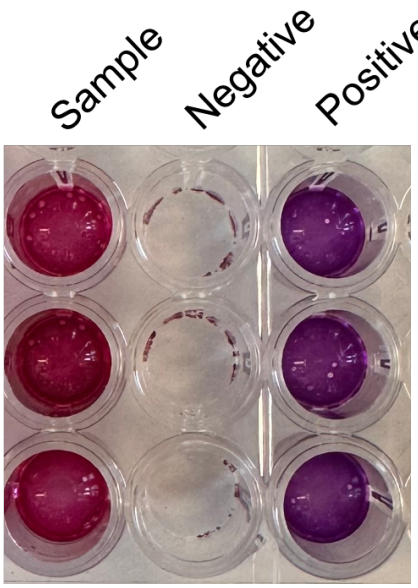

Supplementary Figure 6. Measurement of aldehyde product using Purpald as a purple-color-forming agent. Formaldehyde was used as positive control and for the negative control, cell lysate without expression of BAPAT was used. There was no significant purple product formed in the negative control.

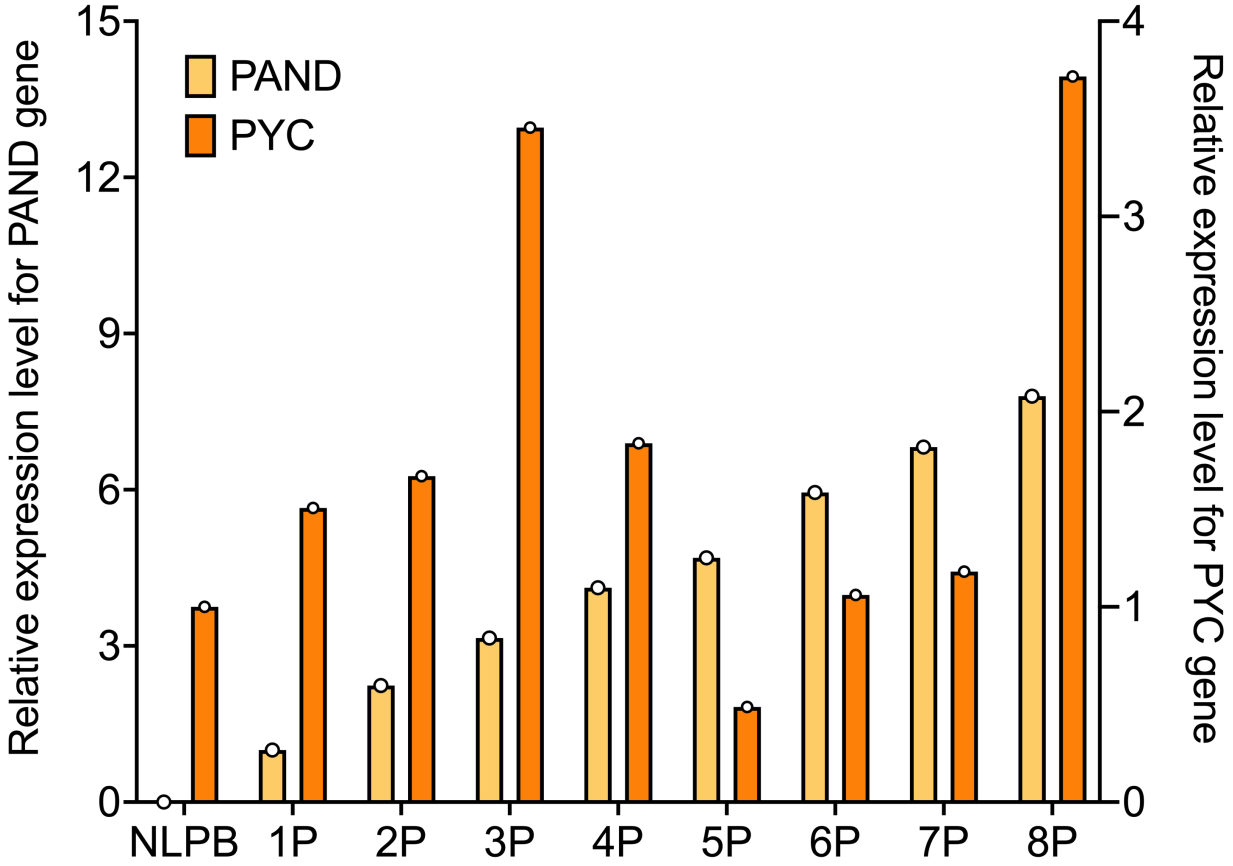

Supplementary Figure 7. qPCR analysis of *PAND* and *PYC* gene expression. Experiment was done with one biological replicate (n =1). Source data for this figure is available in the Source Data file.

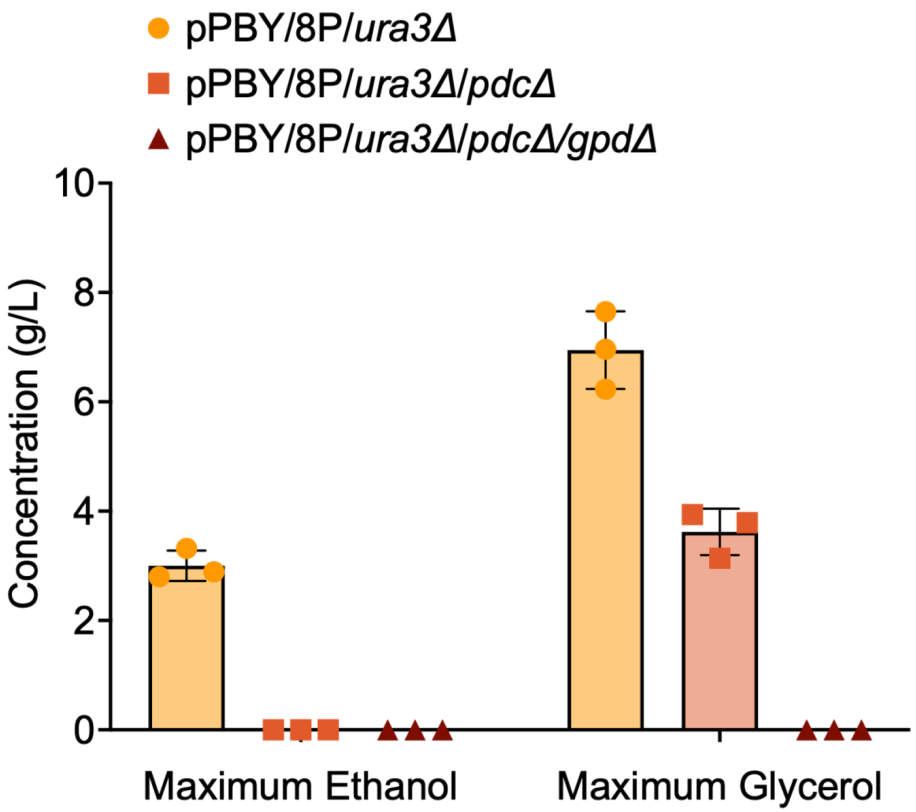

Supplementary Figure 8. Ethanol and glycerol accumulation of three strains, including pPBY/8P/*ura3*Δ, pPBY/8P/*ura3*Δ/*pdc*Δ, pPBY/8P/*ura3*Δ/*pdc*Δ/*gpd*Δ. Data present mean ± S.D. of three biologically independent samples (n = 3). Source data for this figure is available in the Source Data file.

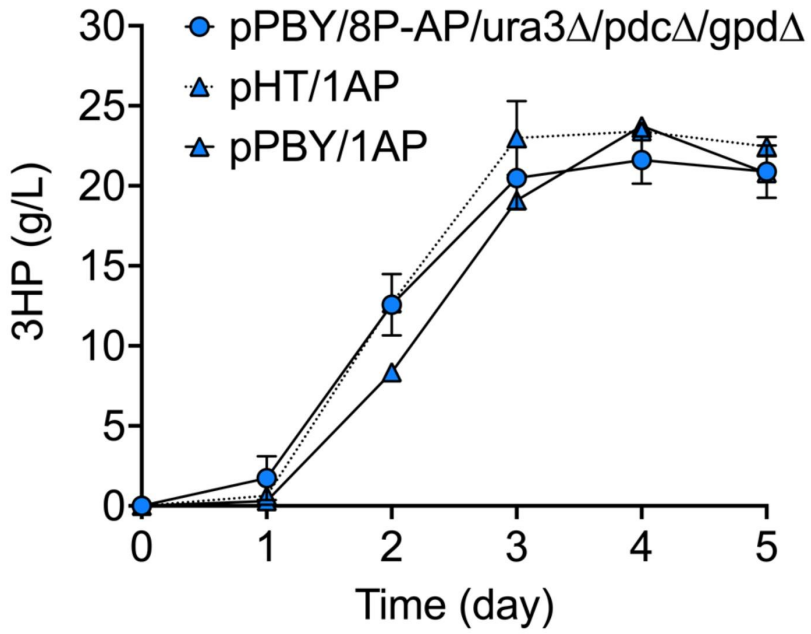

Supplementary Figure 9. 3HP production using pPBY/8P-AP/*ura3*Δ/*pdc*Δ/*gpd*Δ, pHT/1AP/Δ*ura3* and pPBY/1AP/*ura3*Δ. Data present mean ± S.D. of three biologically independent samples (n = 3). Source data for this figure is available in the Source Data file.

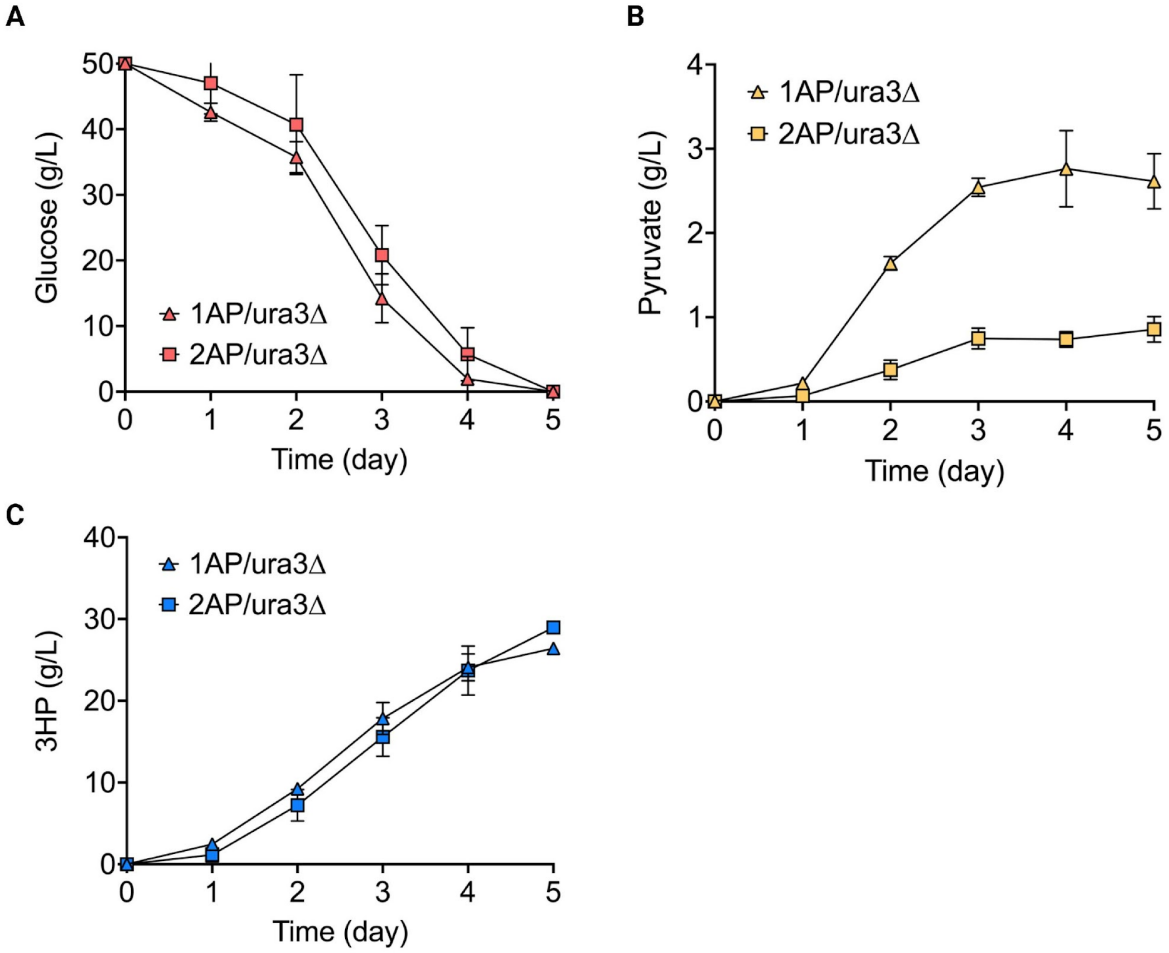

Supplementary Figure 10. Fermentation Profiles of 1AP/ura3Δ and 2AP/ura3Δ Strains in CSM Medium. (A) Glucose consumption, (B) pyruvate accumulation and (C) 3HP production profile of 1AP/*ura3*Δ and 2AP/*ura3*Δ in CSM medium. Data present mean ± S.D. of three biologically independent samples (n = 3). Source data for this figure is available in the Source Data file.

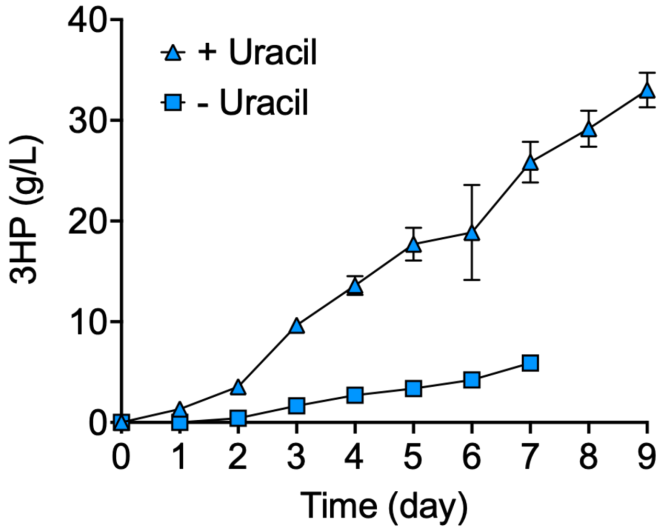

Supplementary Figure 11. 3HP production profile of 2AP/*ura3*Δ in CSL with or without uracil. Data present mean ± S.D. of three biologically independent samples (n = 3). Source data for this figure is available in the Source Data file.

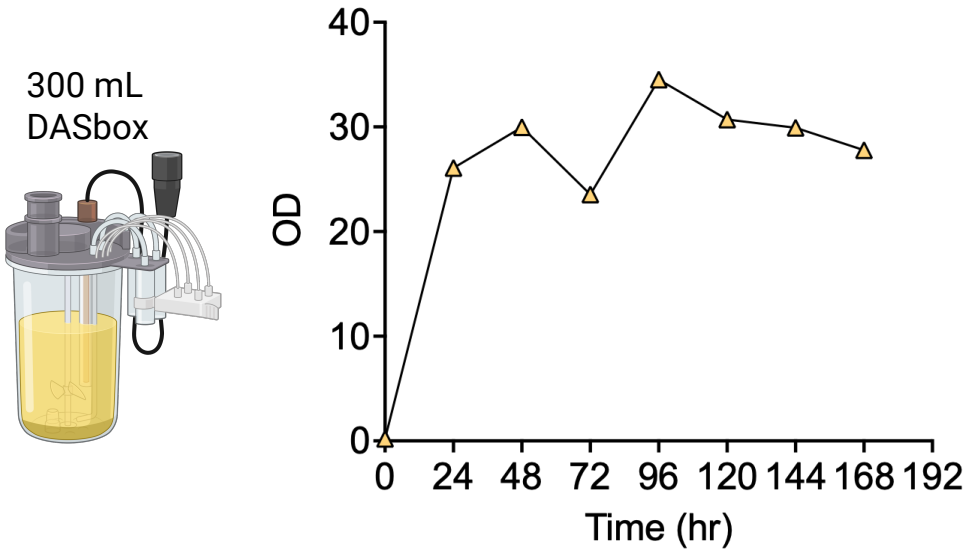

Supplementary Figure 12. Cell growth of 2AP strain in fed-batch fermentation at 300 mL scales using CSL medium. Two independent biological replicates were performed (n = 2) and mean value from two replicate is presented. Source data for this figure is available in the Source Data file. Created in BioRender. Zhao, H. (2025) https://BioRender.com/vkz7w01.

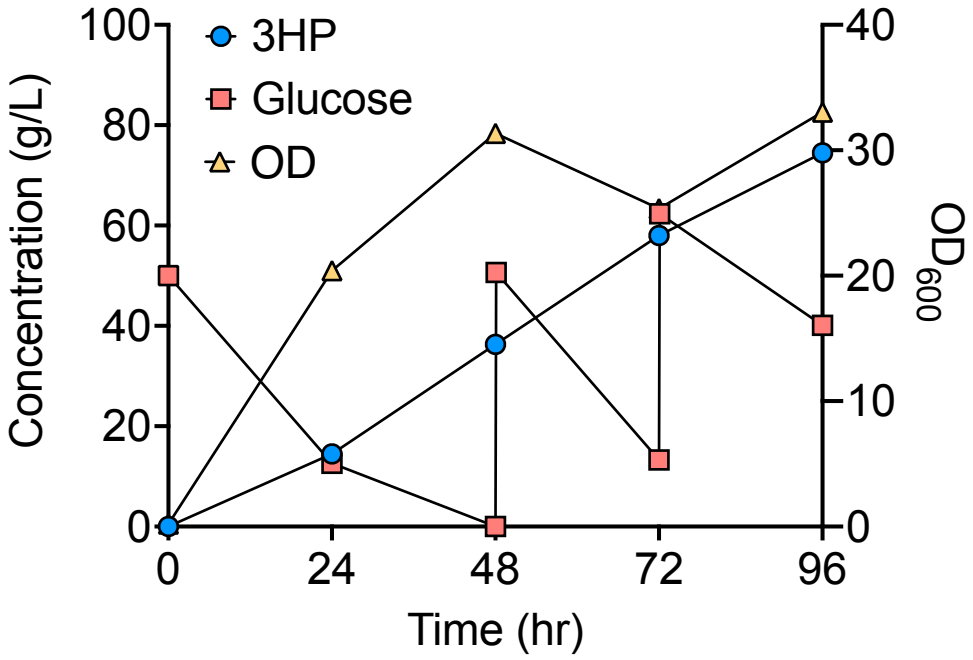

Supplementary Figure 13. Fermentation profile of 2AP in CSL in 3L bioreactor. Experiment was done with one biological replicate (n =1). Source data for this figure is available in the Source Data file.

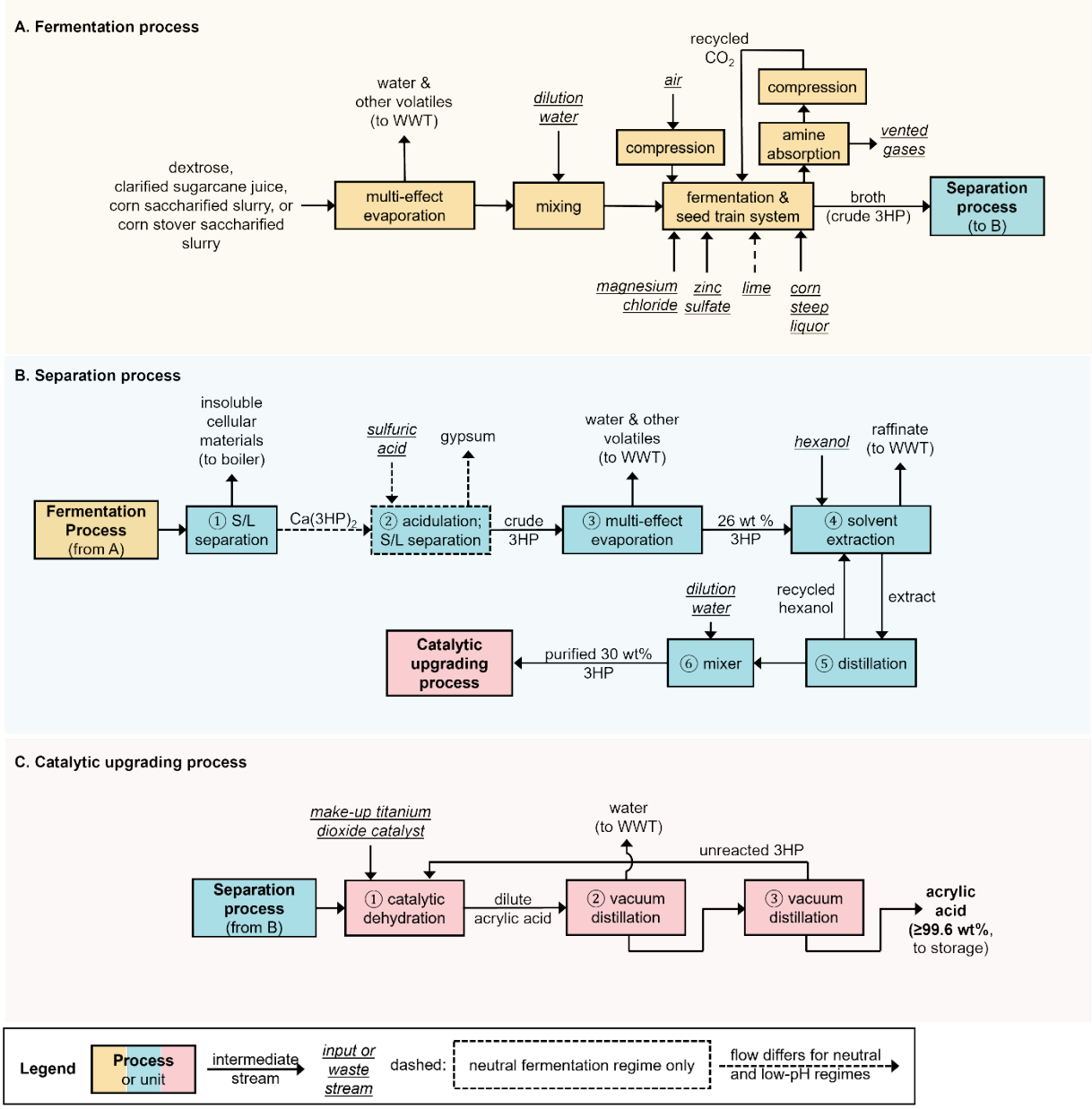

Supplementary Figure 14. Simplified block flow diagrams of the designed biomanufacturing facilities. (A) fermentation, (B) separation, and (C) catalytic upgrading processes for all scenarios. Acronyms denote wastewater treatment (WWT) and solid-liquid separation (S/L separation). While a limited amount of lime is needed under low-pH regimes to maintain a pH of 4.0 (Supplementary Data 1), no sulfuric acid is required and no gypsum is formed (as re-acidulation is not performed) under low-pH regimes. A full process flowsheet is available online[20].

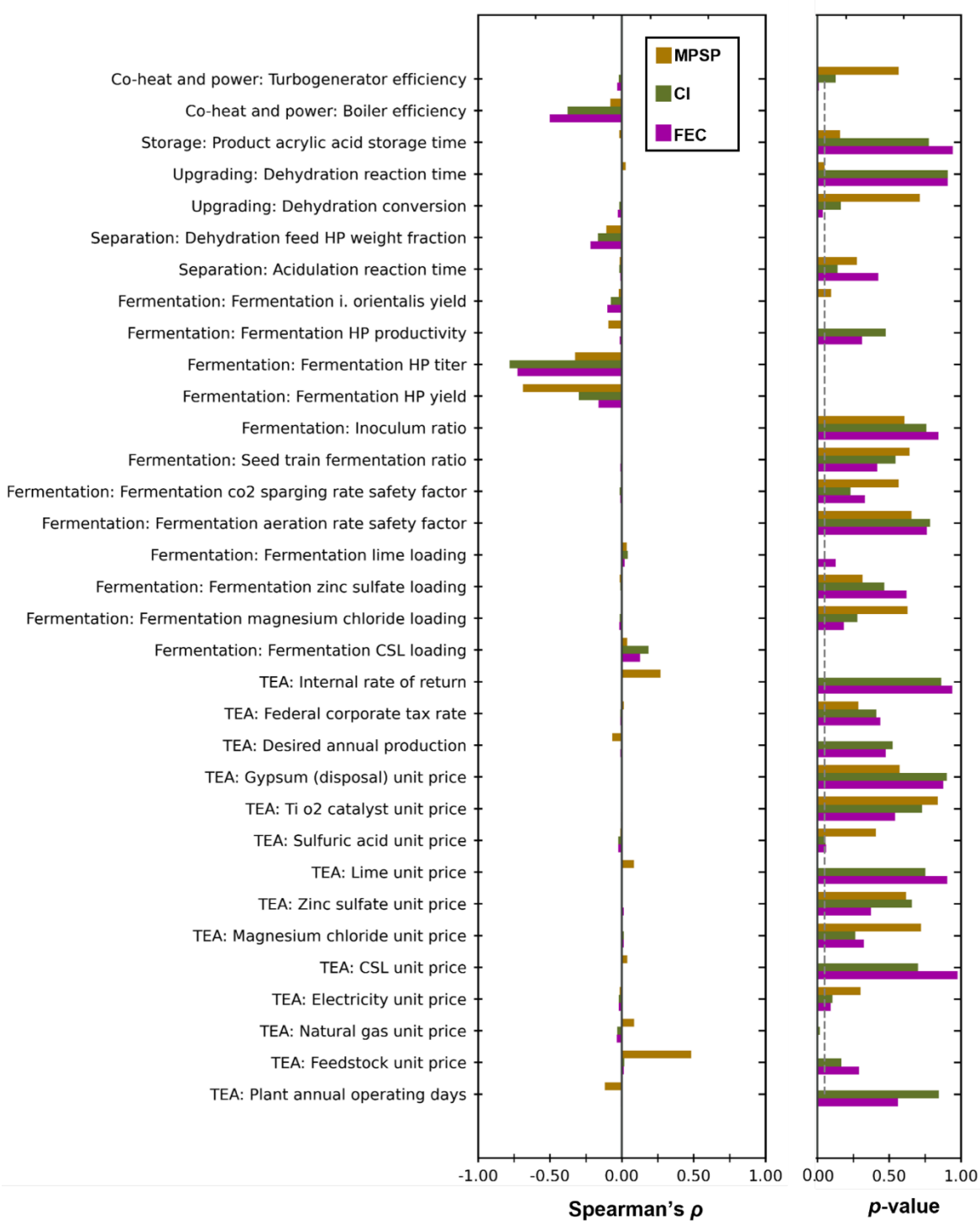

Supplementary Figure 15. Sensitivity analysis results for the biomanufacturing facility in the *dextrose scenario*. Spearman's rank order correlation coefficients (Spearman's ρ; *x*-axis, left; from -1.00 to 1.00) and corresponding *p*-values (*x*-axis, right; from 0.00 to 1.00) for minimum product selling price (MPSP), carbon intensity (CI) and fossil energy consumption (FEC) of acrylic acid (produced via catalytic upgrading of 3HP) with respect to each of 33 parameters included in the uncertainty analysis (*y*-axes). The vertical dashed gray line represents a *p*-value of 0.05. Source data for this figure is available in the Source Data file.

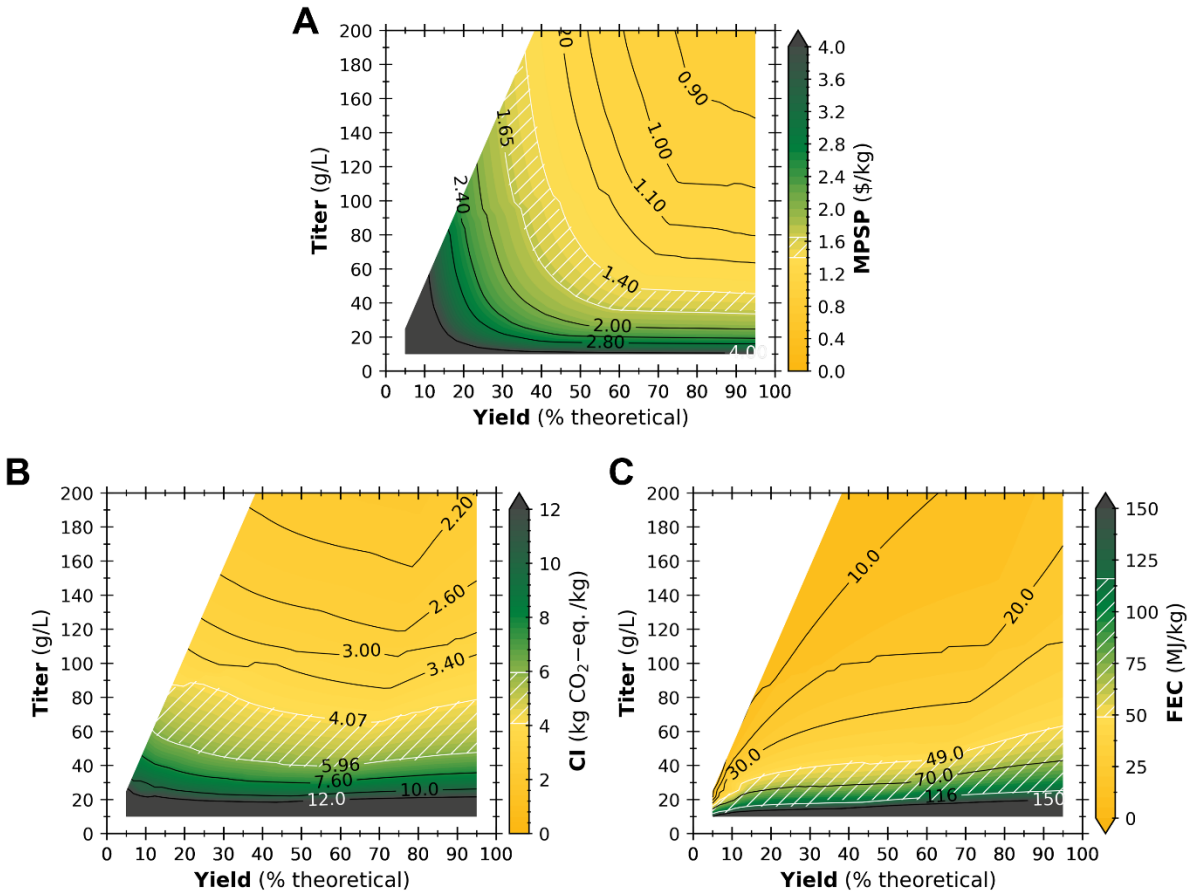

Supplementary Figure 16. Yield–titer landscape of economic and environmental metrics for corn-accepting biomanufacturing. (**A**) Minimum product selling price (MPSP), (**B**) carbon intensity (CI, as 100-year global warming potential), and (**C**) fossil energy consumption (FEC) for corn-accepting biomanufacturing facilities across 3,600 fermentation yield-titer combinations at the baseline productivity (0.548 g/L/h) for low-pH fermentation. Yield is shown as % of the theoretical maximum (%theoretical) scaled to the theoretical maximum yield of 1.00 g/g-glucose-equivalent (based on carbon balance). The hatched region shows the market price range for acrylic acid ($1.40–1.65/kg)[21]. For a given point on the figure, the *x-axis* value represents the yield, the *y-axis* value represents the titer, and the color and contour lines represent the value of MPSP, CI, or FEC. Tabulated data breaking down capital and material costs, heating and cooling duties, electricity consumption, CI, and FEC for each scenario are available online[20]. Source data for this figure is available in the Source Data file.

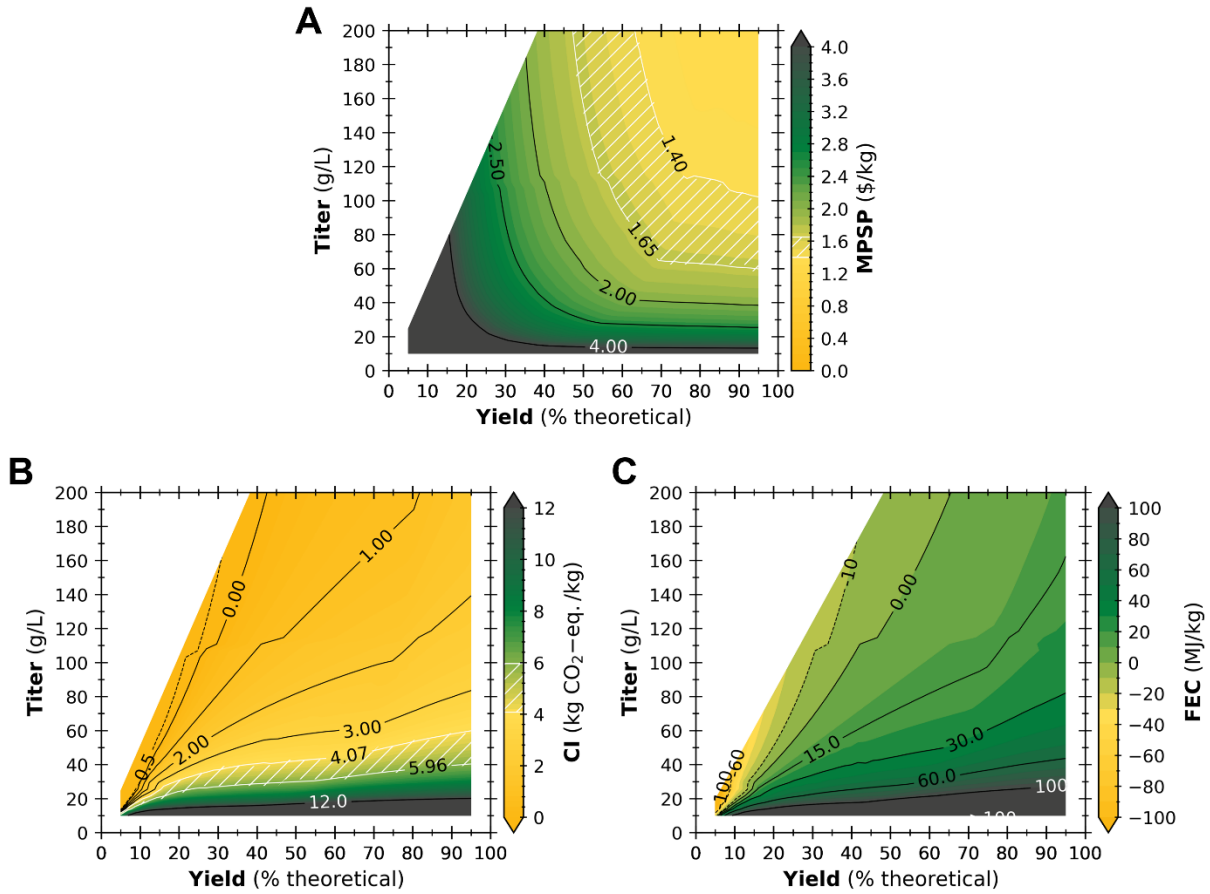

Supplementary Figure 17. Yield–titer landscape of economic and environmental metrics for sugarcane-accepting biomanufacturing. (A) Minimum product selling price (MPSP), (B) carbon intensity (CI, as 100-year global warming potential), and (C) fossil energy consumption (FEC) for sugarcane-accepting biomanufacturing facilities across 3,600 fermentation yield-titer combinations at the baseline productivity (0.548 g/L/h) for low-pH fermentation. Yield is shown as % of the theoretical maximum (%theoretical) scaled to the theoretical maximum yield of 1.00 g/g-glucose-equivalent (based on carbon balance). The hatched region shows the market price range for acrylic acid ($1.40–1.65/kg)[21]. For a given point on the figure, the *x-axis* value represents the yield, the *y-axis* value represents the titer, and the color and contour lines represent the value of MPSP, CI, or FEC. Tabulated data breaking down capital and material costs, heating and cooling duties, electricity consumption, CI, and FEC for each scenario are available online[20]. Source data for this figure is available in the Source Data file.

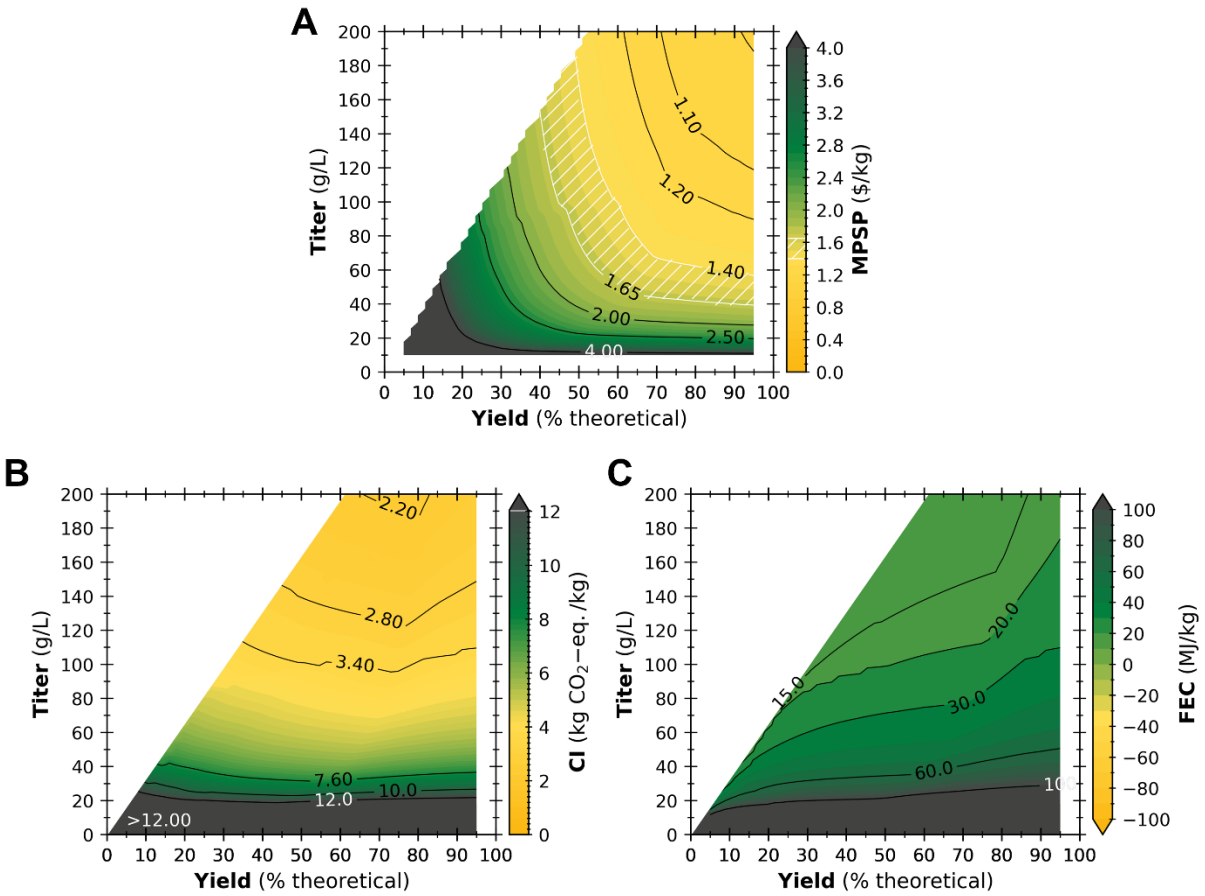

Supplementary Figure 18. Yield–titer landscape of economic and environmental metrics for corn stover-accepting biomanufacturing. (**A**) Minimum product selling price (MPSP), (**B**) carbon intensity (CI, as 100-year global warming potential), and (**C**) fossil energy consumption (FEC) for corn stover-accepting biomanufacturing facilities across 3,600 fermentation yield-titer combinations at the baseline productivity (0.548 g/L/h) for low-pH fermentation. Yield is shown as % of the theoretical maximum (%theoretical) scaled to the theoretical maximum yield of 1.00 g/g-glucose-equivalent (based on carbon balance). The hatched region shows the market price range for acrylic acid ($1.40–1.65/kg)[21]. For a given point on the figure, the *x-axis* value represents the yield, the *y-axis* value represents the titer, and the color and contour lines represent the value of MPSP, CI, or FEC. Tabulated data breaking down capital and material costs, heating and cooling duties, electricity consumption, CI, and FEC for each scenario are available online[20]. Source data for this figure is available in the Source Data file.

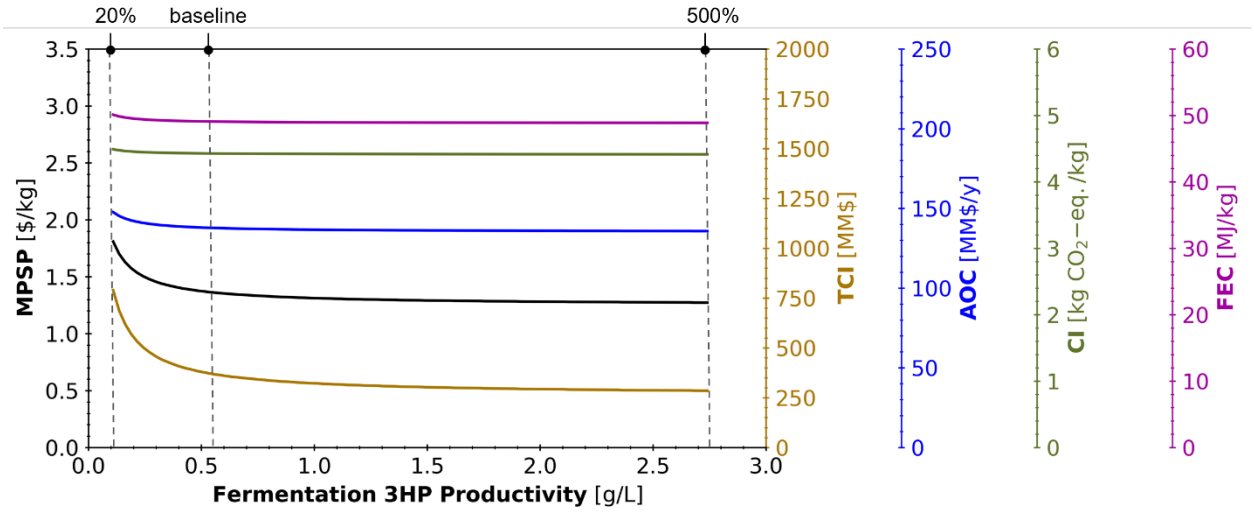

Supplementary Figure 19. Effect of 3HP productivity on economic and environmental metrics in the dextrose scenario. Minimum product selling price (MPSP), total capital investment (TCI), annual operating cost (AOC), carbon intensity (CI; *y*-axes), and fossil energy consumption (FEC) for biorefineries producing acrylic acid (produced via catalytic upgrading of 3HP) in the dextrose scenario at alternative values for fermentation 3HP productivity (*x*-axis). Vertical dashed lines indicate productivity equivalent to 20%, 100%, and 500% of the baseline productivity (0.548 g/L/h). Source data for this figure is available in the Source Data file.

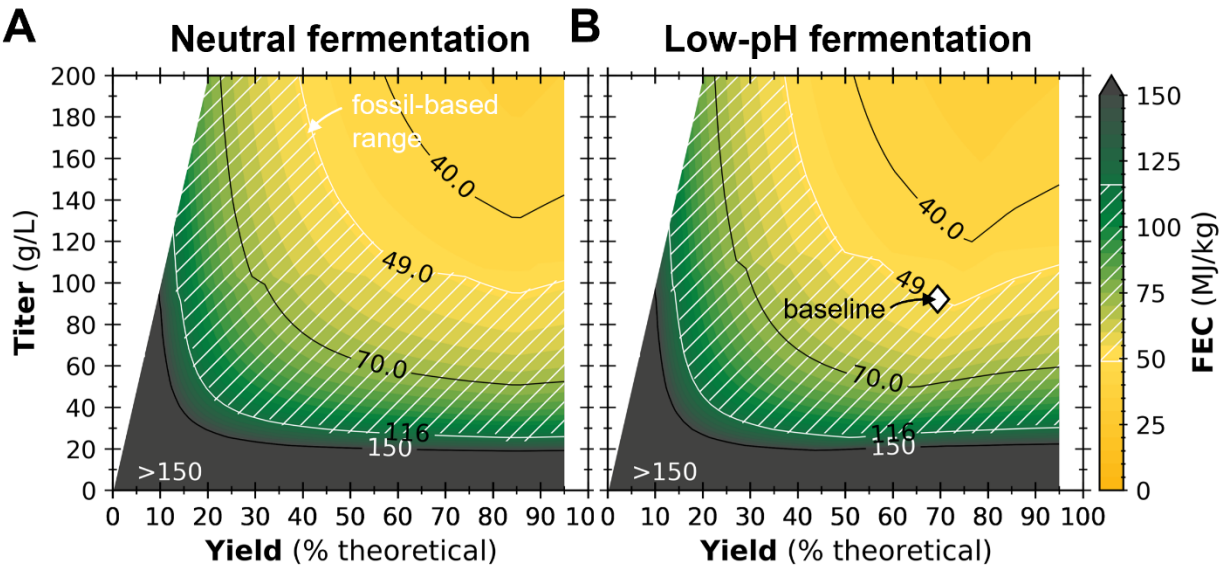

Supplementary Figure 20. Yield–titer landscape of fossil energy consumption (FEC) for neutral and low-pH dextrose fermentation. Fossil energy consumption (FEC) for dextrose-accepting biomanufacturing facilities across 3,600 fermentation yield-titer combinations at the baseline productivity of dextrose scenario (i.e., at a productivity of 0.548 g/L/h) for (A) neutral and (B) low-pH fermentation. Yield is shown as % of the theoretical maximum (%theoretical) scaled to the theoretical maximum yield of 1.00 g/g-glucose-equivalent (based on carbon balance). The hatched region shows a range bounded by FEC values reported for fossil-based acrylic acid[22,23]. For a given point on the figure, the *x-axis* value represents the yield, the *y-axis* value represents the titer, and the color and contour lines represent the value of FEC. Tabulated data breaking down capital and material costs, heating and cooling duties, electricity consumption, CI, and FEC for each scenario are available online[20]. Source data for this figure is available in the Source Data file.

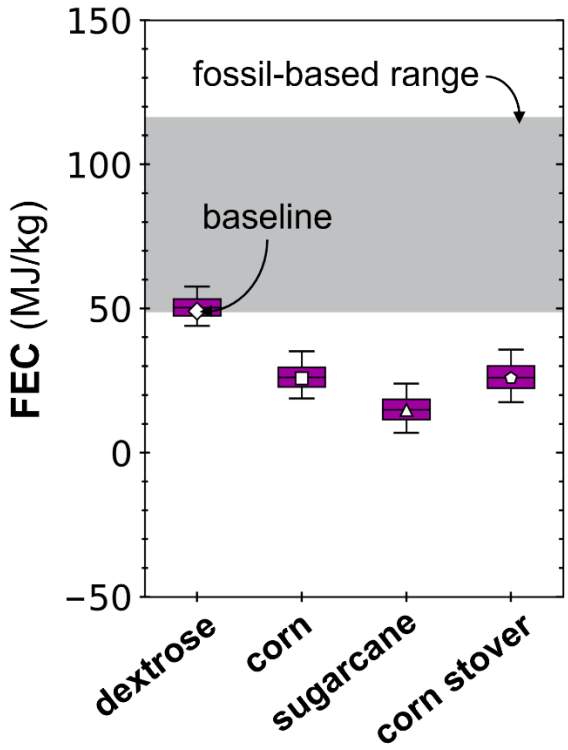

Supplementary Figure 21. Uncertainty analysis of fossil energy consumption for 3HP-derived acrylic acid across four feedstock scenarios. Uncertainties (box-and-whisker plots) for fossil energy consumption (FEC) per kg of acrylic acid produced by catalytic upgrading of 3HP produced via microbial conversion of glucose and sucrose by *I. orientalis*. Box and whisker plots show results for four scenarios (markers report results for baseline values): (i) fermentation performance achieved in the DASbox using dextrose (*dextrose*, diamond markers); (ii) corn-based 3HP biomanufacturing under the same assumptions for fermentation performance as that achieved in the DASbox (*corn*, square markers); (v) sugarcane based 3HP biomanufacturing under the same assumptions for fermentation performance as that achieved in the DASbox (*sugarcane*, triangle markers); and (vi) corn stover based 3HP biomanufacturing under the same assumptions for fermentation performance as that achieved in the DASbox (*corn stover*, pentagon markers; baseline values and distributions for all parameters included in the uncertainty analysis for each scenario are detailed in Supplementary Data 1). On box-and-whisker plots, whiskers, boxes, and the middle line represent 5^{th}/95^{th}, 25^{th}/75^{th}, and 50^{th} percentiles, respectively, from 6000 Monte Carlo simulations for each scenario. respectively, from 5000 Monte Carlo simulations for each scenario. The shaded gray region shows a range bounded by FEC values reported for fossil-based acrylic acid[22,23]. Tabulated data breaking down capital and material costs, heating and cooling duties, electricity consumption, CI, and FEC for each scenario are available online[20]. Source data for this figure is available in the Source Data file.

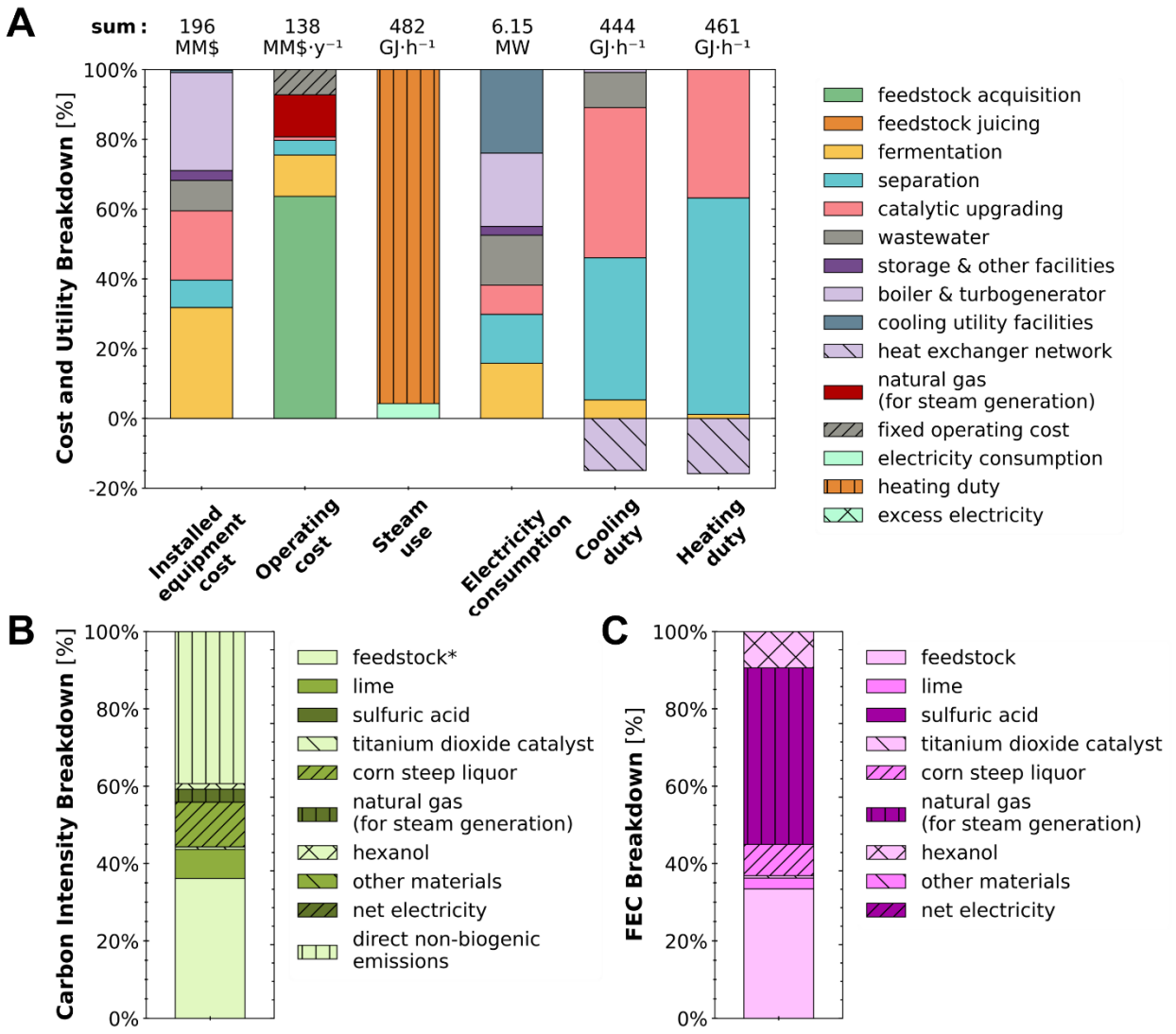

Supplementary Figure 22. Economic and environmental breakdowns for acrylic acid production via dextrose-to-3HP fermentation. Breakdowns for (A) system costs and utility demands, (B) carbon intensity (CI) quantified as 100-year global warming potential (GWP_{100}), and (C) fossil energy consumption (FEC) of acrylic acid produced via fermentation of dextrose to 3HP by engineered *I. orientalis* in the *dextrose scenario*. For the biomanufacturing facility's operating cost ($MM\$ \cdot y^{-1}$), contributions from fixed operating costs, sales revenue from excess electricity, purchase of natural gas for product drying, and material costs by process area are shown. Values above stacked bars are totals including offsets. For heating duty, cooling duty, and electricity consumption, values indicate totals during operation. The biomanufacturing facility is assumed to operate 330 days annually at the baseline condition (baseline values and distributions with literature references for all parameters are detailed in Supplementary Data 1). Tabulated data breaking down capital and material costs, heating and cooling duties, electricity consumption, CI, and FEC are available online[20]. Source data for this figure is available in the Source Data file.

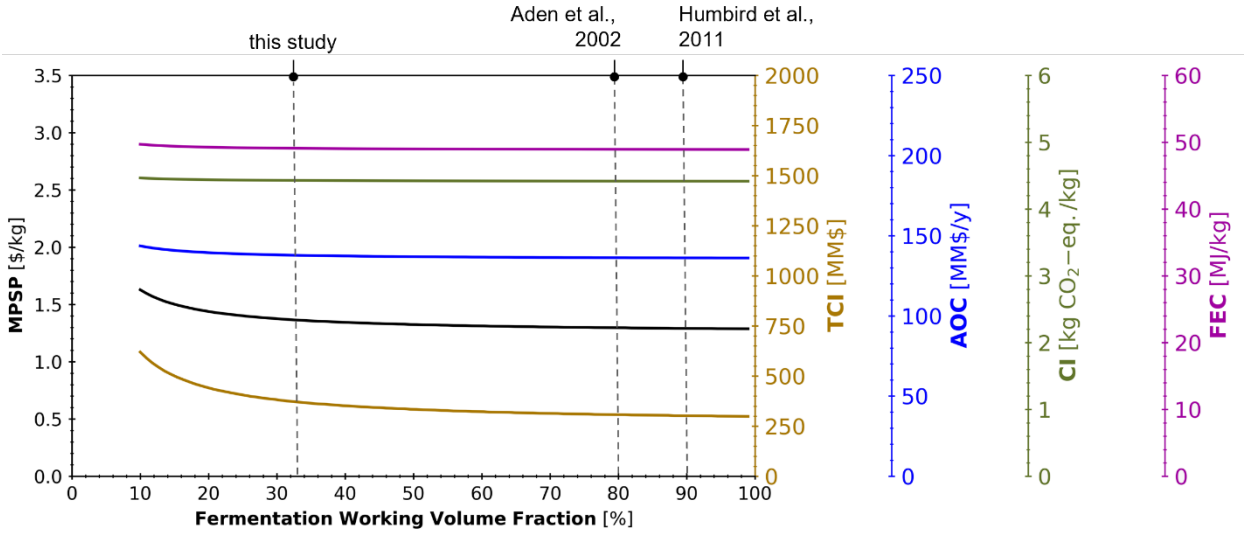

Supplementary Figure 23. Effect of fermentation working volume fraction on economic and environmental metrics in the dextrose scenario. Minimum product selling price (MPSP), total capital investment (TCI), annual operating cost (AOC), carbon intensity (CI; *y*-axes), and fossil energy consumption (FEC) for biorefineries producing acrylic acid (produced via catalytic upgrading of 3HP) in the *dextrose scenario* at alternative values for assumed fermentation working volume fraction (*x*-axis). Vertical dashed lines indicate the fermentation working volume fraction assumed by this study,[3] and [2]. Source data for this figure is available in the Source Data file.

Supplementary References

1. Liu, K., Phillips, J. R., Sun, X., Mohammad, S., Huhnke, R. L., & Atiyeh, H. K. Investigation and modeling of gas-liquid mass transfer in a sparged and non-sparged continuous stirred tank reactor with potential application in syngas fermentation. *Fermentation* 5, 75 (2019).
2. Humbird, D., Davis, R., Tao, L., Kinchin, C., Hsu, D., Aden, A., Schoen, P., Lukas, J., Olthof, B., Worley, M., Sexton, D., & Dudgeon, D. Process design and economics for biochemical conversion of lignocellulosic biomass to ethanol: dilute-acid pretreatment and enzymatic hydrolysis of corn stover. http://www.nrel.gov/docs/fy11osti/47764.pdf (2011).
3. Aden, A., Ruth, M., Ibsen, K., Jechura, J., Neeves, K., Sheehan, J., Wallace, B., Montague, L., Slayton, A., & Lukas, J. Lignocellulosic biomass to ethanol process design and economics utilizing co-current dilute acid prehydrolysis and enzymatic hydrolysis for corn stover. NREL/TP-510-32438 https://docs.nrel.gov/docs/fy02osti/32438.pdf (2002).
4. Zallot, R., Oberg, N., & Gerlt, J. A. The EFI web resource for genomic enzymology tools: leveraging protein, genome, and metagenome databases to discover novel enzymes and metabolic pathways. *Biochemistry*, 58(41), 4169-4182 (2019).
5. Zhao, P., Ma, C., Xu, L. & Tian, P. Exploiting tandem repetitive promoters for high-level production of 3-hydroxypropionic acid. *Appl Microbiol Biotechnol* **103**, 4017–4031 (2019).
6. Kim, J. W., Ko, Y.-S., Chae, T. U. & Lee, S. Y. High-level production of 3-hydroxypropionic acid from glycerol as a sole carbon source using metabolically engineered *Escherichia coli*. *Biotechnol. Bioeng.* **117**, 2139–2152 (2020).
7. Zhang, Y., Su, M., Chen, Y., Wang, Z., Nielsen, J., & Liu, Z. Engineering yeast mitochondrial metabolism for 3-hydroxypropionate production. *Biotechnol. Biofuels Bioprod.* **16**, 64 (2023).
8. Yu, W., Cao, X., Gao, J. & Zhou, Y. J. Overproduction of 3-hydroxypropionate in a super yeast chassis. *Bioresour. Technol.* **361**, 127690 (2022).
9. Qin, N., Li, L., Wan, X., Ji, X., Chen, Y., Li, C., Liu, P., Zhang, Y., Yang, W., Jiang, J., Xia, J., Shi, S., Tan, T., Nielsen, J., Chen, Y., & Liu, Z. Increased CO_2 fixation enables high carbon-yield production of 3-hydroxypropionic acid in yeast. *Nat. Commun.* **15**, 1591 (2024).
10. Wu, X., Cai, P., Gao, L., Li, Y., Yao, L., & Zhou, Y. J. Efficient bioproduction of 3-hydroxypropionic acid from methanol by a synthetic yeast cell factory. *ACS Sustain. Chem. Eng.* **11**, 6445–6453 (2023).
11. Liu, D., Hwang, H. J., Otoupal, P. B., Geiselman, G. M., Kim, J., Pomraning, K. R., Kim, Y. M., Munoz, N., Nicora, C. D., Gao, Y., Burnum-Johnson, K. E., Jacobson, O., Coradetti, S., Kim, J., Deng, S., Dai, Z., Prahl, J. P., Tanjore, D., Lee, T. S., Magnuson, J. K., & Gladden, J. M. Engineering *Rhodosporidium toruloides* for production of 3-hydroxypropionic acid from lignocellulosic hydrolysate. *Metab. Eng.* **78**, 72–83 (2023).
12. Gao, J., Yu, W., Li, Y., Jin, M., Yao, L., & Zhou, Y. J. Engineering co-utilization of glucose and xylose for chemical overproduction from lignocellulose. *Nat. Chem. Biol.* **19**, 1524–1531 (2023).
13. Kang, F., Gu, F., Zhong, Y., Cui, Z., Liang, Q., & Qi, Q. Expanding the genetic toolkit of *Yarrowia lipolytica*: dynamic promoter engineering enables high-titer biosynthesis of 3-hydroxypropionic acid. *Bioresour. Technol*. (2025).
14. Borodina, I., Kildegaard, K. R., Jensen, N. B., Blicher, T. H., Maury, J., Sherstyk, S., Schneider, K., Lamosa, P., Herrgård, M. J., Rosenstand, I., Öberg, F., Forster, J., & Nielsen, J. Establishing a synthetic pathway for high-level production of 3-hydroxypropionic acid in *Saccharomyces cerevisiae* via β-alanine. *Metab. Eng.* **27**, 57–64 (2015).
15. Batista, R. S., Chaves, G. L., Oliveira, D. B., Pantaleão, V. L., dos Santos Neves, J. D., & da Silva, A. J. Glycerol as substrate and NADP+-dependent glyceraldehyde-3-phosphate dehydrogenase enable higher production of 3-hydroxypropionic acid through the β-alanine pathway in *E. coli*. *Bioresour. Technol.* **393**, 130142 (2024).
16. Xiao, H., Shao, Z., Jiang, Y., Dole, S. & Zhao, H. Exploiting *Issatchenkia orientalis* SD108 for succinic acid production. *Microb. Cell Fact.* **13**, 121 (2014).
17. Fatma, Z., Tan, S. I., Boob, A. G. & Zhao, H. A landing pad system for multicopy gene integration in *Issatchenkia orientalis*. *Metab. Eng.* **78**, 200–208 (2023).

18. Tran, V., Fatma, Z., Song, X. & Zhao, H. Development of a CRISPR/Cas9-based tool for gene deletion in *Issatchenkia orientalis*. *mSphere* **4**, (2019).
19. Tran, V. G., Mishra, S., Bhagwat, S. S., Shafaei, S., Shen, Y., Allen, J. L., Crosly, B. A., Tan, S. I., Fatma, Z., Rabinowitz, J. D., Guest, J. S., Singh, V., & Zhao, H. An end-to-end pipeline for succinic acid production at an industrially relevant scale using *Issatchenkia orientalis*. *Nat. Commun.* **14**, 6152 (2023).
20. BioSTEAM Development Group. 3-Hydroxypropionic Acid Biorefineries. https://github.com/BioSTEAMDevelopmentGroup/Bioindustrial-Park/tree/master/biorefineries/HP (2024).
21. IHS Markit. Chemical Economics Handbook - Acrylic Acid and Esters. IHS Markit, London, England. (2020).
22. Wang, M., Elgowainy, A., Lu, Z., Bafana, A., Benavides, P. T., Burnham, A., Cai, H., Dai, Q., Gracida, U., Hawkins, T. R., Jaquez, P. V., Kelly, J. C., Kwon, H., Lee, U., Liu, X., Ou, L., Sun, P., Winjobi, O., Xu, H., Yoo, E., Zaimes, G. G., & Zang, G. Greenhouse gases, regulated emissions, and energy use in technologies model. Computer Software. USDOE Office of Energy Efficiency and Renewable Energy (EERE). (2020).
23. Wernet, G., Bauer, C., Steubing, B., Reinhard, J., Moreno-Ruiz, E., & Weidema, B. The ecoinvent database version 3 (part I): overview and methodology. *The Int. J. Life Cycle Assess.* **21**, 1218–1230 (2016).